Effect of P/Bi substitution on optical and thermal properties of Ga-Ge-Se-Te glasses

R. Golovchak[a], M.J. Seage[a], J. Szlęzak[b,c], Y. Shpotyuk[b,d,*], D. Płoch[b], F. Cheviré[c], C. Boussard-Pledel[c], B. Bureau[c]

[a] *Department of Physics, Engineering and Astronomy, Austin Peay State University, Clarksville, TN 37044, USA*

[b] *Institute of Physics, University of Rzeszow, Rzeszow, 35-959, POLAND*

[c] *Univ Rennes, CNRS, ISCR [(Institut des Sciences Chimiques de Rennes)] – UMR 6226, F-35000 Rennes, FRANCE*

[d] *Department of sensor and semiconductor electronics, Ivan Franko National University of Lviv, Lviv 79017, UKRAINE*

**corresponding author: yashpotyuk@gmail.com*

ABSTRACT

Novel P-containing bulk $Bi_xGa_5Ge_{20}P_{10-x}Se_{45}Te_{20}$ glasses have been successfully fabricated and studied with optical spectroscopy and differential scanning calorimetry. Non-isothermal and isothermal crystallization kinetics are investigated, and anti-Arrhenius behavior is observed for the crystallization of some phases in x = 1 glass. The thermal stability of the glass is shown to decrease with an increase in Bi concentration, whereas as the concentration of P increases, the glass stability increases and the glass does not crystallize during regular DSC heating scans. It is found that substitution of P with Bi in glass composition leads to a decrease in the optical gap and increase in its density.

Keywords: Chalcogenide glass; Crystallization; Kinetics; DSC; Optical properties

1. Introduction

Tellurium- and selenium-based glass matrices have been shown to be suitable for many applications in modern photonics, combining high IR transparency (up to ~18 μm), excellent fiber drawing capability, large optical nonlinearities and good solubility of various dopants [1-4]. The latter allows further enhancement of the intrinsic physical properties of these materials through the nanoscale design. In particular, several chemical elements (Bi, Sb, rare earth, Ga) are shown to modify these glasses at the nanoscale, leading to significant changes in their electrical conductivity [5,6], thermo-electric behavior [7-10], phase-change memory effect [11,12], potential to host low-dimensional quantum systems [13-16], unique optical properties [1,17], and other interesting phenomena. The combination of all these features makes chalcogenide alloys modified at nanoscale a very appealing multifunctional medium for numerous applications, including (nano)optics and (nano)electronics [9-19]. The progress in such applications depends on our ability to fabricate ordered regions of desired size and concentration in the amorphous matrix of chalcogenide glasses by modifying the technological process of their synthesis or using external influences, such as thermal treatment (crystallization above the glass transition temperature), photo-exposure (laser-induced fluidity, local melting) or others. Among all dopants, Ga and Bi look especially attractive for nanoscale modification. The Ga is usually added to a chalcogenide glass matrix in order to improve solubility of rare-earth elements [20,21], while Bi is known to be a unique dopant in chalcogenide glasses (which normally are highly insensitive to metal doping and possess *p*-type conductivity) capable of unpinning the Fermi level and thus changing the conduction from *p*- to *n*-type [5,6]. Moreover, Bi-doped nanostructured glasses are capable of strong thermo-electric effect [7,9], whereas Bi-based crystals (Bi_2Te_3 and Bi_2Se_3) have been proven to possess topological insulator properties [14] – a

new state of matter in which gapless surface states reside in the bulk insulating gap of the materials and are protected by the topology.

Despite all of these advantages, the incorporation of Ga and Bi into the structure of Ge-Se-Te glasses significantly decreases their thermal stability [22,23]. In this work, we added P to stabilize the vitreous matrix and increase the thermal stability of Bi- and Ga-modified Ge-Se-Te glasses within $Bi_xGa_5Ge_{20}P_{10-x}Se_{45}Te_{20}$ family. Optical properties and crystallization kinetics in these complex metamaterials are investigated by optical spectroscopy and differential scanning calorimetry (DSC) techniques.

2. Materials and methods

The $Bi_{10}Ga_5Ge_{20}Se_{45}Te_{20}$ (RP-0), $Bi_7Ga_5Ge_{20}P_3Se_{45}Te_{20}$ (RP-3), $Bi_5Ga_5Ge_{20}P_5Se_{45}Te_{20}$ (RP-5), $Bi_3Ga_5Ge_{20}P_7Se_{45}Te_{20}$ (RP-7), $Bi_1Ga_5Ge_{20}P_9Se_{45}Te_{20}$ (RP-9) and $Ga_5Ge_{20}P_{10}Se_{45}Te_{20}$ (RP-10) glasses were prepared by conventional melt-quenching technique. The appropriate amount of high-purity (5N or more) Ga, Bi, P, Ge, Se and Te precursors (~20 g in total) were vacuum-sealed in silica tube (10 mm diameter), heated up to 900 °C, homogenized for ~10 hours at 800 °C in a rocking furnace, and quenched into room-temperature water from 650 °C. To relieve the mechanical strains, each as-quenched glass was annealed at ~30 °C below the corresponding glass transition temperature for 3 h. Then, the ingots were cut (and polished when necessary) for the measurements.

The overall glassy state of the obtained materials was confirmed by the absence of crystalline reflexes in the X-ray diffraction (XRD) patterns of as-prepared samples (Fig. 1) studied using X-ray diffractometer PANalytical X'Pert Pro (Cu Kα radiation with λ=1.5418 Å).

The homogeneity and actual compositions of the prepared $Bi_xGa_5Ge_{20}P_{10-x}Se_{45}Te_{20}$ (x=0,1,3,5,7,10) glasses were verified by scanning electron microscopy (SEM) with energy-dispersive X-ray analysis (EDX) using FEI Helios NanoLab 650 microscope. No significant deviations (more than ±2 at.%) from nominal compositions have been found, and no significant inhomogeneities have been detected through SEM.

DSC measurements were performed using a NETZSCH DSC-204 F1 instrument calibrated with a set of standard elements. Bulk ~10 mg chunks of each glass were heated in 40 μl aluminum crucibles under nitrogen atmosphere at q = 2, 5, 10, 15, and 20 K/min constant heating rates. The DSC scan protocol included two runs at every q: the first run revealed a glass-to-supercooled liquid transition and crystallization peaks, while the second one of a fully crystallized sample provided a confident baseline and a check of completeness of crystallization processes. The samples with x < 5 were additionally studied using isothermal crystallization protocol, where the samples were heated with q = 30 K/min to a certain crystallization temperature (T_c) above T_g and maintained there for several hours. To assure the repeatability of the results, the DSC measurements were repeated minimum three times for each heating rate or crystallization temperature, and for each composition, using a fresh sample for every measurement. The crystallization peaks were fitted with Fraser-Suzuki distributions [24]:

$$y = a_0 \exp\left[-\ln 2 \left(\frac{\ln\left(1 + 2a_3 \frac{x - a_1}{a_2}\right)}{a_3} \right)^2 \right] \quad (1)$$

where a_0, a_1, a_2, and a_3 are the amplitude, position, half-width and asymmetry of the $y(x)$ curve, respectively. The number of the peaks (distributions) in the envelope of the fitted experimental

DSC curve was determined by the goodness of the fit. The fitting, integration and normalization were done using Origin software.

Optical transmission spectra in Vis/NIR region were taken with a PerkinElmer LAMBDA 950 spectrophotometer. The MIR and FIR optical transmission was recorded with a Bruker Vertex 70V spectrometer. The Vis/NIR spectra were used for optical gap estimation with the aid of PARAV software [25].

3. Results and discussion

Optical properties of the investigated P-containing glasses are consistent with those of the same family chalcogenides [23,26,27]. Optical transmittance window extends from ~2 up to ~16 μm (Fig. 2a), showing some absorption bands in ~2-4 μm range caused by the atmospheric contaminations (water vapor and CO_2, on the first hand), weak impurity absorption line at ~4.5 μm due to Se-H vibrations [28], and a broad ~8-11 μm absorption feature of complex origin. The latter includes contributions from oxygen-containing impurity complexes (P-O, Ge-O) [28,29], as well as possible intrinsic absorption from mixed P-Ga-Ge environment [30]. The apparent longwave shift of multiphonon cut-off is due to a substitution of P by heavier Bi in the composition. Optical transmission in the fundamental optical absorption edge region was used to calculate the absorption coefficient (Fig. 2b) and estimate the optical gap (Table 1) using Tauc plot and PARAV program [25]. The obtained data show that substitution of P with Bi in glass composition leads to a decrease in optical gap values (Table 1), as was also observed previously in similar Bi-contaning glasses [23]. It is interesting to note, though, that estimated optical gap values of the investigated P-containing glasses are comparable with those of isocompositional

Sb-containing ones (Table 1, values in square brackets) [23], preserving a general trend on Bi concentration dependence (RP-0 sample being opaque). So, it can be concluded that Sb and P both have smaller impact on the optical gap, than Bi content. The glass transition temperature, T_g, on the other hand, decreases by ~15 K when Sb is substituted with P in the composition (Table 1). At the same time, T_g values as determined from DSC heating curves show very weak dependence on Bi or P content (T_g = 215±3 ^{o}C for 10 K/min runs, see Table 1), which is consistent with previous observations in Sb-containing glass system [23].

DSC thermograms of the investigated P-containing glasses recorded at different heating rates q = 2, 5, 10, 15, 20, 30 K/min (Fig. 3) may be used also to estimate the activation energy of viscous flow, E_{Tg}, by, for example, Ozawa method [31,32]. As it is obvious from the obtained results, the thermally annealed (structurally relaxed) samples do not show any strong compositional dependence of E_{Tg}, except for RP-10 sample with most P content where E_{Tg} has its maximum value (Table 1). The density measured by Archimedes' method, on the other hand, decreases by ~5-8 % when Sb is substituted with P, and shows a strong dependence on Bi, increasing with Bi content in both families (Table 1).

The onset temperature of the glass transition T_g^{on} and the peak temperature of the first crystallization process T_c (both values determined from 10 K/min DSC runs) can be used to calculate Dietzel criterion of glass stability $\Delta T = T_c - T_g^{on}$ [33]. The calculations show that Dietzel criterion generally increases with substitution of Sb or Bi with P, losing its meaning for the glasses with P content more than 5 at.% ($x < 5$) due to the disappearance of crystallization peaks in DSC heating mode. So, we can conclude, that higher P content in the composition leads to enhanced stability of the glass phase depressing nucleation and crystal growth processes. On the other hand, the density of glass increases and the glass becomes less stable (smaller ΔT

values) when Sb or P is substituted with Bi (Table 1), the most unstable being the RP-0 composition with 10 at.% of Bi content (it's still in overall amorphous state, though, according to XRD data, Fig. 1).

For the samples with higher Bi content (x > 5) two families of crystallization peaks are observed, which merge into a single broad complex crystallization peak for RP-5 glass (Fig. 4). The RP-7, RP-9 and RP-10 samples do not show considerable crystallization peaks during regular DSC heating scans (the system is not allowed enough time for nucleation and further crystal growth processes), but crystallization can be observed using isothermal DSC mode (Fig. 4). Fraser-Suzuki fits (1) of non-isothermal and isothermal DSC curves (Fig. 5) suggest crystallization of at least five phases for RP-0 glass (which may contain pre-existing nuclei and Bi-based nanocrtystallites), three for RP-3, RP-5, RP-7 and RP-9 glasses each, and two in the case of RP-10 sample. It should be noted, that shape of real crystallization peaks can be more complicated than Fraser-Suzuki form (1) depending on the nature of the crystallizing phase, but such a fit is considered the best estimate to determine crystallization temperatures and activation energies of overlapped crystallization processes of unknown nature.

The estimated activation energies (E_a) of crystallization are presented in Table 2 for all resolved peaks. In the case of non-isothermal crystallization, the ln (q) *vs* $10^3/T_c$ dependences were used, while for isothermal kinetics the activation energies were estimated using ln (t_c) *vs* $10^3/T_i$ dependences (t_c is the time of the crystallization peak occurring at T_i isothermal temperature). Although at this point it is not possible to derive strict compositional regularities, because it is not obvious that all numbered peaks in Table 2 represent the same crystallizing phases in different samples, some conclusions can still be drawn. First of all, the replacement of Bi with P in composition (compare RP-0 and RP-10 glasses) leads to a decrease in the number of

crystallizing phases and drop (almost twice) in the crystallization activation energy values. Glasses having both chemical elements in their structure demonstrate even smaller values of activation energies for crystallization (like RP-7 sample, Table 2). Such trend can be explained by an overall shift of the crystallization process to lower temperatures (as one goes from RP-5 to RP-0 glass), where higher viscosity of supercooled liquid imposes more constraints on structural rearrangements needed for crystallization to occur. A very distinct behaviour has been recorded for crystallization activation energies of RP-9 glass (Table 2): two (for peaks I and II) out of three appear to be negative (anti-Arrhenius behaviour). This is manisfested in DSC isothermal scans as anomalous time shift of the exothermic crystallization peak with the increase in the crystallization (annealing) temperature. Normally, when isothermal annealing temperature increases, the crystallization starts at earlier times (as it is indeed observed in Fig. 4 for RP-7, RP-10 samples and peak III of RP-9 sample shown by "Arrhenius" arrow). However, the opposite behavior is observed for peaks I and II of RP-9 sample: when the crystallization temperature increases during isothermal DSC scans, the crystallization occurs at later times (shown by "anti-Arrhenius" arrow in Fig. 4 for RP-9 sample) which is unusual.

Negative apparent activation energy of crystallization is an interesting phenomenon observed in some polymer glass-formers, which is associated with interplay between the free energy of nuclei formation and activation energy for diffusion across the phase boundary [34]. According to the nucleation theory proposed by Turnbull and Fisher [35] and discussed comprehensively by Wunderlich [36], the temperature dependence of the nucleation rate r is given by:

$$r = r_0 e^{-\left(\frac{E_d}{RT} + \frac{\Delta F}{RT}\right)} \quad (2)$$

where r_0 is the preexponential factor, E_d is the activation energy for diffusion across the phase boundary, and ΔF is the maximum free energy needed for nucleus formation.

The ΔF and E_d exponential terms in (2) have opposite effects on the nucleation rate. The value of E_d is considered to be approximately constant [37], whereas ΔF is inversely proportional to the degree of supercooling [34]:

$$\Delta F \sim \frac{1}{\left(T - T_m\right)^2} \tag{3}$$

According to (3), the value of ΔF increases drastically when T approaches melting point T_m. In this case, the overall crystallization rate would be determined by the nucleation rate, which temperature dependence is controlled by the temperature variation of ΔF. As it is evident from (3), ΔF decreases when temperature departs from T_m, that causes ΔF exponential term in (2) to increase, which, in turn, gives rise to the crystallization rate in close proximity to T_m [34]. This anti-Arrhenius behavior yields a negative value of the experimental (apparent) activation energy for the phases, which crystallization temperature is close to the melting point T_m [34]. We believe, this is also a reason for irregular (complex and barely reprodicible) shape of crystallization peak observed for RP-9 glass at the crystallization temperature 405 ^{o}C after 40 min (Fig. 4). After ΔF drops below a certain value at further temperature decrease, the E_d exponential term in (2) becomes dominant, and then the nucleation rate is controlled by a transport process, which obeys regular Arrhenius temperature dependence. So, the negative values of apparent activation energies for crystallization observed for peaks I and II of RP-9 glass can be explained by a close proximity of the crystallizing phases to their corresponding

melting points, where crystallization rate is determined by the temperature dependence of free energy needed for nucleus formation.

The nature of these phases requires further thorough investigations using combination of Raman/IR spectrocopy, electron microscopy, XRD analysis, and such complementary structural probes as X-ray photoelectron spectroscopy and extended X-ray absorption fine structure spectroscopy.

4. Conclusions

The optical transmittance window of $Bi_xGa_5Ge_{20}P_{10-x}Se_{45}Te_{20}$ (x=0,1,3,5,7) glasses ranges from ~2 μm to ~16 μm. Substitution of P with Bi leads to an increase in density of the glass, a decrease in the estimated optical gap of these materials and, finally, to the complete opacity in Vis-IR of ~2 mm thick sample with 10 at.% of Bi. Stability of the glass increases with P addition, and crystallization does not occur during regular DSC heating scans (q > 5 K/min) in the samples with x < 5. Non-isothermal and isothermal crystallization kinetics analyzed with Frazer-Suzuki fit function reveals negative apparent activation energy for crystallization of two phases in x = 1 (RP-9) sample. This anti-Arrhenius behaviour is explained by a dominant role of free energy of nucleus formation in the crystallization rate if crystallization occurs in a close proximity to melting points of these phases. The activation energies of crystallization for the glasses with both P and Bi in their network are smaller than for the edge compositions with only Bi or P. This is consistent with the idea that increase in E_a can be caused by a shift of the crystallization processes to lower temperatures. Owing to the obtained results, the developed P-

containing glass matrix can be considered as a good candidate for fiber drawing, which can be used in IR optics, photonics and sensor applications.

Acknowledgements

This research is supported by POLONIUM common action program for years 2018–2019 realized in respect to bilateral Agreement on scientific-technical cooperation between Polish and French governments. RG and YS are grateful to Erasmus+ program for the support of this research.

References

[1] J-L. Adam, X. Zhang (Eds), Chalcogenide Glasses: Preparation, properties and application, Woodhead Publishing series in Electronic and Optical Materials No.44, 2014.

[2] A. Feltz, Amorphous inorganic materials and glasses, VCH Publishers, New York, 1993.

[3] A. Zakery, S.R. Elliott, Optical nonlinearities in chalcogenide glasses and their applications, Springer-Verlag, Berlin, Heidelberg, 2007.

[4] J.S. Sanghera, I.D. Aggarwal, Active and passive chalcogenide glass optical fibers for IR applications: a review, J. Non-Cryst. Solids 256&257 (1999) 6-16.

[5] C. Vautier, Role of metal impurity “Bi” in amorphous chalcogenide semiconductors, Solid State Phenom. 71 (2000) 249-270.

[6] G. Singh, J. Sharma, A. Thakur, N. Goyal, G. S. S. Saini, S. K. Tripathi, Effect of bismuth on the electrical properties of a-$Ge_{20}Se_{80}$ glasses, J. Optoel. Adv. Mater. 7 (2005) 2069-2076.

[7] Y. Liu, Sh. Yuan, J. Xie, F. Shangguan, J. Ren, G. Chen, A Study on Crystallization Kinetics of Thermoelectric Bi_2Se_3 Crystals in Ge–Se–Bi Chalcogenide Glasses by Differential Scanning Calorimeter, J. Am. Ceram. Soc. 96, *7* (2013) 2141–2146.

[8] J.-F. Li, W.-S. Liu, L.-D. Zhao, M. Zhou, High-performance nanostructured thermoelectric materials, NPG Asia Mater. 2, *4* (2010) 152–158.

[9] B. Srinivasan, C. Boussard-Pledel, V. Dorcet, M. Samanta, K. Biswas, R. Lefèvre, F. Gascoin, F. Cheviré, S. Tricot, M. Reece, B. Bureau, Thermoelectric Properties of Highly-Crystallized Ge-Te-Se Glasses Doped with Cu/Bi, Materials 10 (2017) 328.

[10] B. Srinivasan, A. Gellé, F. Gucci, C. Boussard-Pledel, B. Fontaine, R. Gautier, J.-F. Halet, M. Reece, B. Bureau, Realizing a Stable High Thermoelectric zT ~2 over a Broad Temperature Range in $Ge_{1-x-y}Ga_xSb_yTe$ via Band Engineering and Hybrid Flash-SPS Processing, Inorg. Chem. Front. 6 (2019) 63-73.

[11] J.L. Bosse, I. Grishin, Y.G. Choi, B.-Ki Cheong, S. Lee, O.V. Kolosov, B.D. Huey, Nanosecond switching in GeSe phase change memory films by atomic force microscopy, Appl. Phys. Let. 104 (2014) 053109.

[12] L. Wang, C. D. Wright, M.M. Aziz, C.-Hui Yang, G.-Wei Yang, Design of an optimised readout architecture for phase-change probe memory using $Ge_2Sb_2Te_5$ media, Japanese J. Appl. Phys. 53 (2014) 028002.

[13] H. Lin et al, Chalcogenide glass-on-graphene photonics, Nature Photon. 11 (2017) 798–805.

[14] H. Zhang, C.-X. Liu, X.-L. Qi, X. Dai, Zh. Fang, Sh.-Ch. Zhang, Topological insulators in Bi_2Se_3, Bi_2Te_3 and Sb_2Te_3 with a single Dirac cone on the surface, Nature Physics 5 (2009) 438-442.

[15] L.-X. Qin, X.-C. Pan, F.-Q. Song, L. Zhang, Zh.-H. Sun, M.-Q. Li, P. Gao, B.-C. Lin, S.-M. Huang, R. Zhu, J. Xu, F. Lin, H.-Z. Lu, D. Yu, Zh.-M. Liao, Confined-path interference suppressed quantum correction on weak antilocalization effect in a $BiSbTeSe_2$ topological insulator, Appl. Phys. Lett. 112 (2018) 032102.

[16] N.P. Mitchell, L.M. Nash, D. Hexner, A.M. Turner, W.T. M. Irvine, Amorphous topological insulators constructed from random point sets, Nature Physics 14 (2018) 380–385.

[17] R. Golovchak, Ya. Shpotyuk, J. Szlęzak, A. Dziedzic, A. Ingram, J. Cebulski, Giant VIS-IR light attenuation effect in nanostructured narrow-bandgap glasses, Opt. Lett. 43 (2018) 387-390.

[18] B. J. Eggleton, B. Luther-Davies, K. Richardson, Chalcogenide photonics, Nature Photonics 5 (2011) 141–148.

[19] S. Cui, R. Chahal, Ya. Shpotyuk, C. Boussard, J. Lucas, F. Charpentier, H. Tariel, O. Loreal, V. Nazabal, O. Sire, V. Monbet, Z. Yang, P. Lucas, B. Bureau, Selenide and telluride glasses for mid-infrared bio-sensing, Proc. SPIE, 8938 (2014) 893805-1-9.

[20] M. Scheffler, J. Kirchhof, J. Kobelke, K. Schuster, A. Schwuchow, Increased rare earth solubility in As–S glasses, J. Non-Cryst. Solids 256&257 (1999) 59.

[21] Y.G. Choi, K.H. Kim, B.J. Lee, Y.B. Shin, Y.S. Kim, J. Heo, Emission properties of the Er^{3+}: $^4I_{11/2} \rightarrow {}^4I_{13/2}$ transition in Er^{3+}- and Er^{3+}/Tm^{3+}-doped Ge–Ga–As–S glasses, J. Non-Cryst. Solids 278 (2000) 137.

[22] L. Saturday, C. Johnson, A. Thai, J. Szlęzak, Ya. Shpotyuk, R. Golovchak, Devitrification of Bi- and Ga-containing germanium-based chalcogenide glasses, J. Alloys Compd. 674 (2016) 207-217.

[23] R. Golovchak, A. Kozdras, T. Hodge, J. Szlęzak, C. Boussard-Pledel, Ya. Shpotyuk, B. Bureau, Optical and thermal properties of Sb/Bi-modified mixed Ge-Ga-Se-Te glasses, J. Alloys and Compounds 750 (2018) 721-728.

[24] A. Perejon, P.E. Sanchez-Jimenez, J.M. Criado, L.A. Perez-Maqueda, Kinetic Analysis of Complex Solid-State Reactions, A New Deconvolution Procedure, J. Phys. Chem. B 115 (2011) 1780–1791.

[25] A. Ganjoo, R. Golovchak, Computer program PARAV for calculating optical constants of thin films and bulk materials: Case study of amorphous semiconductors, J. Optoelectron. Adv. Mater. 10, 6 (2008) 1328-1332.

[26] Ya. Shpotyuk, C. Boussard-Pledel, V. Nazabal, R. Chahal, J. Ari, B. Pavlyk, J. Cebulski, J.L. Doualan, B. Bureau, Ga-modified As_2Se_3–Te glasses for active applications in IR photonics, Optical Materials 46 (2015) 228–232.

[27] N. Abdellaoui, F. Starecki, C. Boussard-Pledel, Y. Shpotyuk, J-L. Doualan, A. Braud, E. Baudet, P. Nemec, F. Cheviré, M. Dussauze, B. Bureau, P. Camy, V. Nazabal, Tb^{3+} doped $Ga_5Ge_{20}Sb_{10}Se_{65-x}Te_x$ (x = 0-37.5) chalcogenide glasses and fibers for MWIR and LWIR emissions, Opt. Mater. Express 8 (2018) 2887–2900.

[28] V.S. Shiryaev, E.V. Karaksina, M.F. Churbanov, T.V. Kotereva, B.S. Stepanov, L.A. Ketkova, I.I. Evdokimov, V.V. Koltashev, V.G. Plotnichenko, A.I. Filatov, I.N. Antonov, Special pure germanium-rich Ga-Ge-As-Se glasses for active mid-IR fiber optics, Mater. Res. Bul. 107 (2018) 430-437.

[29] A.M. Efimov, IR fundamental spectra and structure of pyrophosphate glasses along the $2ZnO\text{-}P_2O_5\text{-}2Me_2O\text{-}P_2O_5$ join (Me being Na and Li), J. Non-Cryst. Solids 209 (1997) 209–226.

[30] D.C. Harris, Durable 3–5 μm transmitting infrared window materials, Infrared Phys. & Tech. 39 (1998) 185–201.

[31] T. Ozawa, Nonisothermal kinetics of crystal growth from pre-existing nuclei, Bull. Chem. Soc. Jpn. 57 (1984) 639-643.

[32] T. Ozawa, A new method of analyzing thermogravinetric data, Bull. Chem. Soc. Japan 38 (1965) 1881-1886.

[33] A. Dietzel, Glass Structure and Glass Properties, Glasstech. Ber. 22 (1968) 41-50.

[34] S. Vyazovkin, N. Sbirrazzuoli, Isoconversional Analysis of the Nonisothermal Crystallization of a Polymer Melt, Macromol. Rapid Commun. 23 (2002) 766–770.

[35] J. C. Fisher, D. Turnbull, Rate of Nucleation in Condensed Systems, J. Chem. Phys. 17 (1949) 71.

[36] B. Wunderlich, Macromolecular Physics, Vol. 2, Academic Press, New York, 1976.

[37] J. Schultz, Polymer Material Science, Prentice Hall: Engelwood Cliffs,1974.

Figure Captions

Fig. 1. XRD patterns of the investigated $Bi_xGa_5Ge_{20}P_{10-x}Se_{45}Te_{20}$ glasses.

Fig. 2. Optical transmission (a) and absorption coefficient (b) spectra of $Bi_xGa_5Ge_{20}P_{10-x}Se_{45}Te_{20}$ glasses (RP-0 sample is not shown due to its complete opacity in this optical region).

Fig. 3. DSC scans at different heating rates for $Bi_xGa_5Ge_{20}P_{10-x}Se_{45}Te_{20}$ glasses, showing glass transition region.

Fig. 4. Non-isothermal (RP-0, RP-3, RP-5) and isothermal (RP-7, RP-9, RP-10) DSC scans for $Bi_xGa_5Ge_{20}P_{10-x}Se_{45}Te_{20}$ glasses, showing crystallization.

Fig. 5. Example of Fraser-Suzuki fittings for non-isothermal (RP-0, RP-3, RP-5) and isothermal (RP-7, RP-9, RP-10) crystallization DSC curves of $Bi_xGa_5Ge_{20}P_{10-x}Se_{45}Te_{20}$ glasses.

Table 1. Dietzel criterion of glass stability $\Delta T = T_c - T_g^{on}$ [30], calculated for the investigated $Bi_xGa_5Ge_{20}P_{10-x}Se_{45}Te_{20}$ glasses using DSC curves recorded at 10 K/min heating rate (T_c is the peak value of the earliest crystallization peak, T_g^{on} is the onset value of glass transition); density ρ; estimated optical gap E_g; and estimated activation energies of viscous flow E_{Tg}, averaged for Ozawa's plots of onset and midpoint T_g values. Corresponding values of the same parameters determined for isocompositional $Bi_xGa_5Ge_{20}Sb_{10-x}Se_{45}Te_{20}$ glasses [23] are given in square brackets for comparison.

Parameter Sample	T_g^{on}, °C (±1)	T_c, °C (±1)	ΔT, °C (±1)	E_{Tg}, kJ/mol (±50)	E_g, eV (±0.05)	ρ, g/cm^3 (±0.005)
$Bi_{10}Ga_5Ge_{20}Se_{45}Te_{20}$	218	261	43	280	n/a	5.441
$Bi_7Ga_5Ge_{20}P_3Se_{45}Te_{20}$	217	301	84	270	0.69	5.212
$Bi_5Ga_5Ge_{20}P_5Se_{45}Te_{20}$	215 [229]	357	142 [74]	280	0.76 [0.71]	5.042 [5.226]
$Bi_3Ga_5Ge_{20}P_7Se_{45}Te_{20}$	214 [228]	n/a	n/a [118]	270	0.80 [0.80]	4.858 [5.100]
$Bi_1Ga_5Ge_{20}P_9Se_{45}Te_{20}$	213 [230]	n/a	n/a [143]	270	0.91 [0.85]	4.671 [5.043]
$Ga_5Ge_{20}P_{10}Se_{45}Te_{20}$	215 [231]	n/a	n/a [150]	400	1.01 [1.00]	4.575 [4.983]

Table 2. Average activation energy of crystallization E_a calculated for the investigated materials using Ozawa's plots [28,29].

Sample / E_a	Peak I kJ/mole (±5)	Peak II kJ/mole (±5)	Peak III kJ/mole (±5)	Peak IV kJ/mole (±5)	Peak V kJ/mole (±5)
$Bi_{10}Ga_5Ge_{20}Se_{45}Te_{20}$	271	283	300	228	242
$Bi_7Ga_5Ge_{20}P_3Se_{45}Te_{20}$	266	217	189		
$Bi_5Ga_5Ge_{20}P_5Se_{45}Te_{20}$	142	145	178		
$Bi_3Ga_5Ge_{20}P_7Se_{45}Te_{20}$	102	112	128		
$Bi_1Ga_5Ge_{20}P_9Se_{45}Te_{20}$	-90	-136	116		
$Ga_5Ge_{20}P_{10}Se_{45}Te_{20}$	142	144			

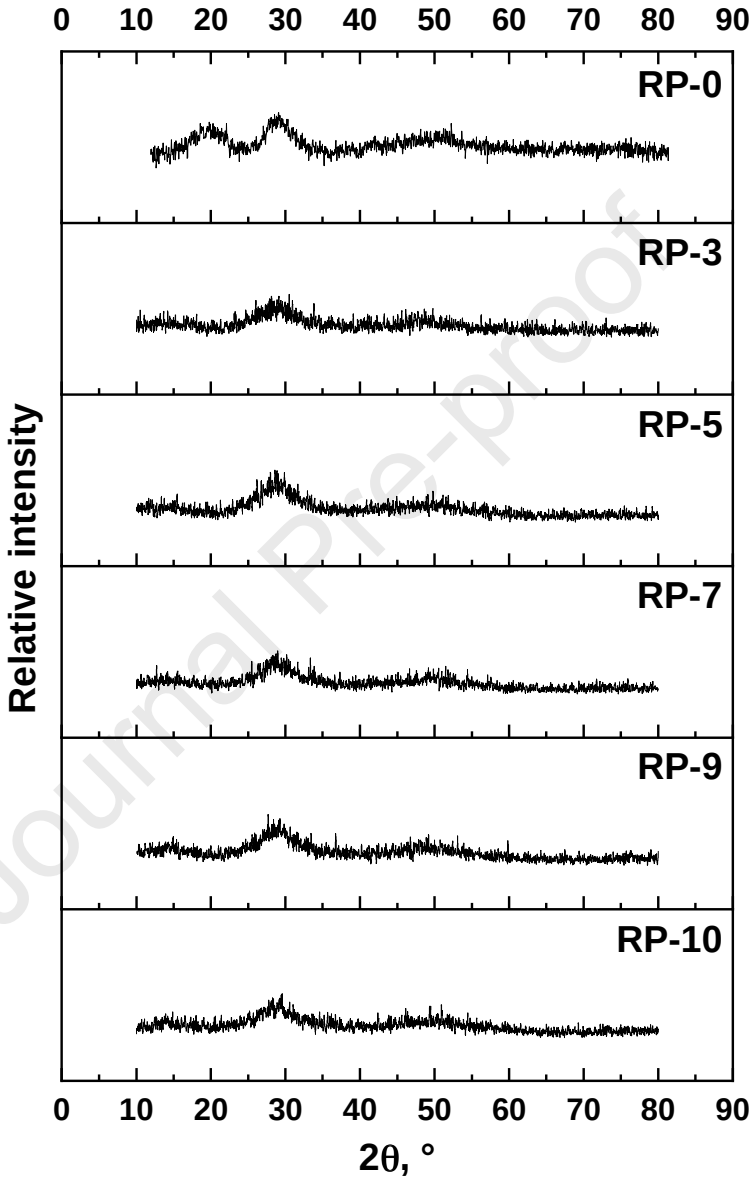

Fig. 1.

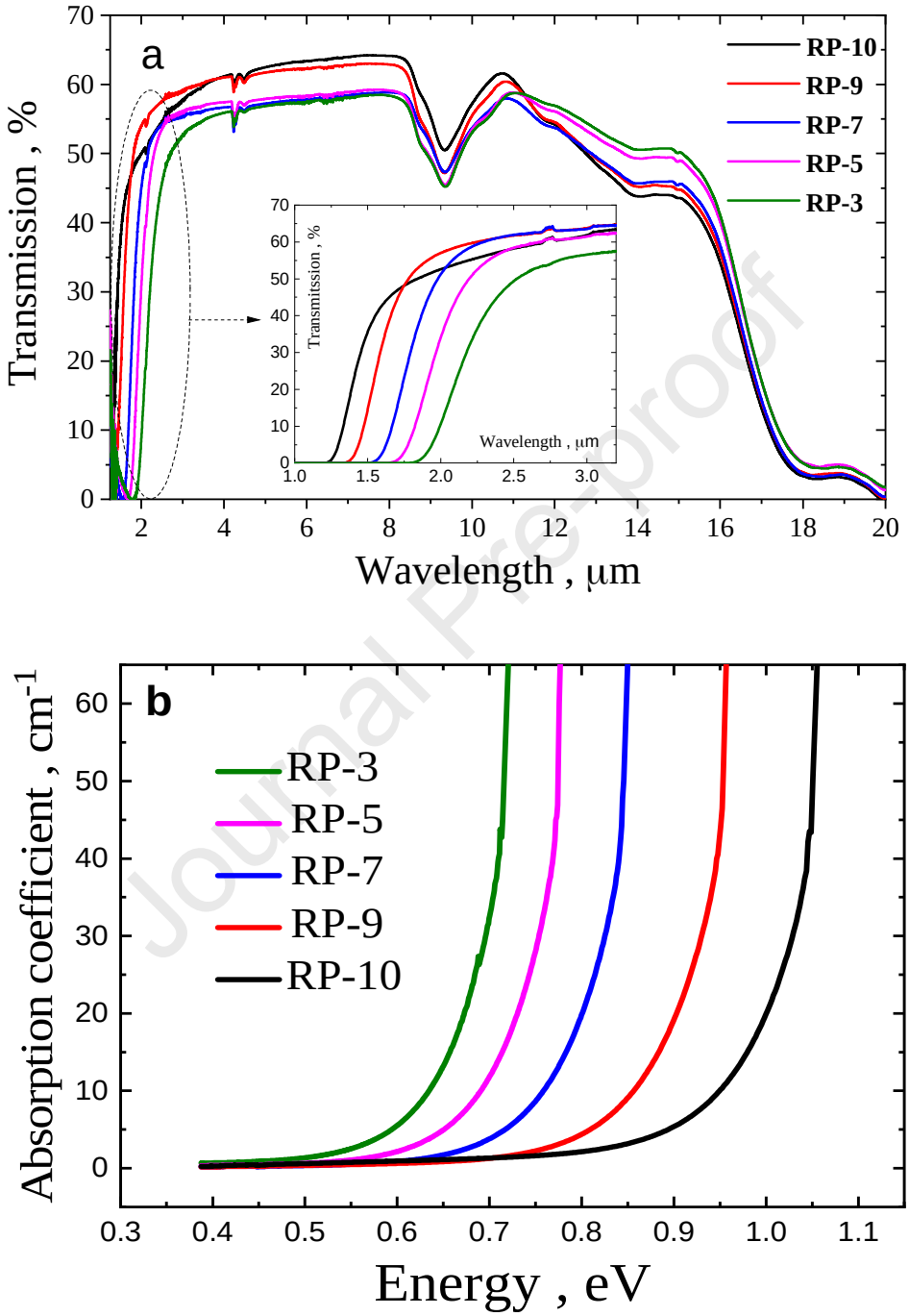

Fig. 2.

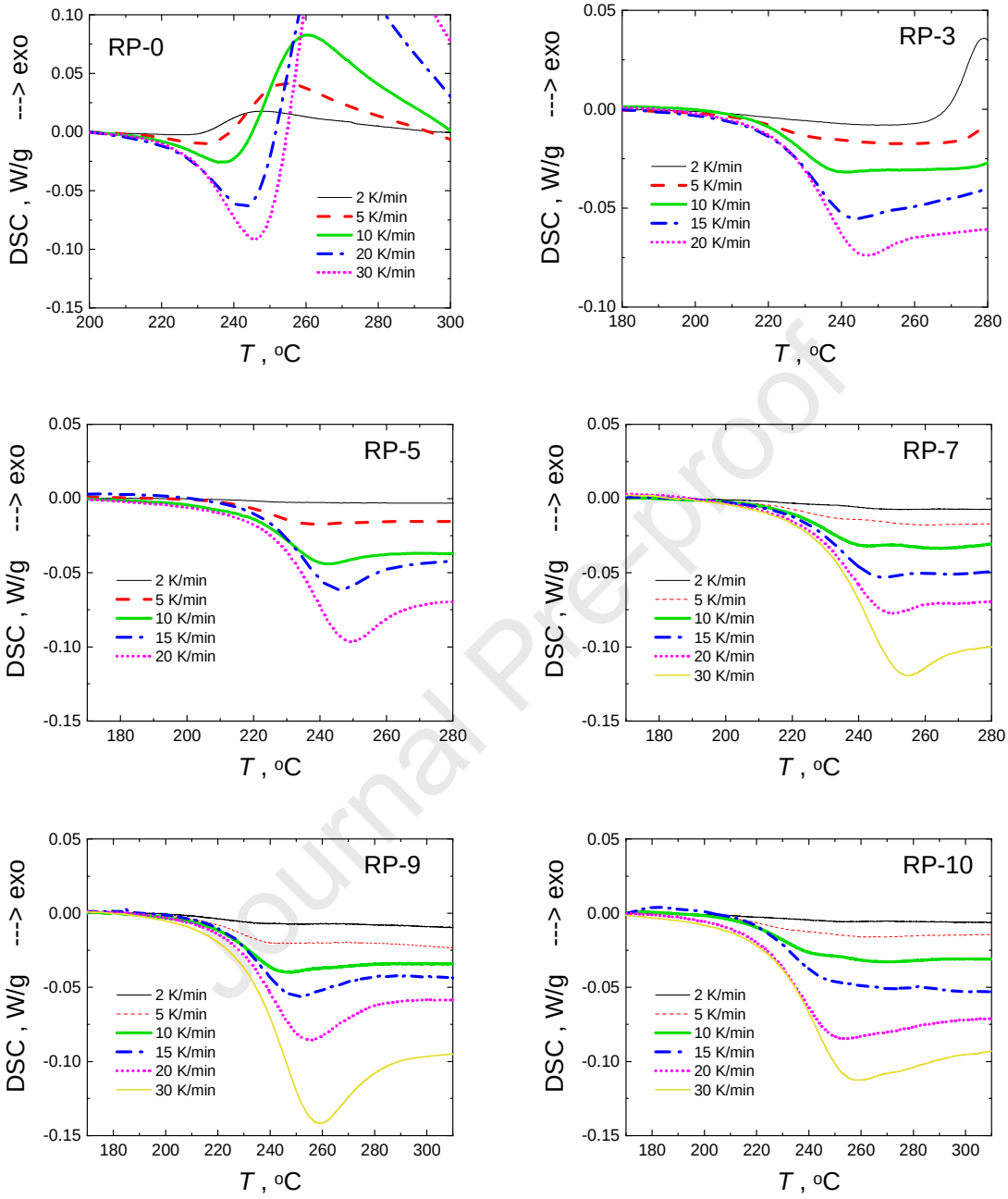
RP-0
RP-3
RP-5
RP-7
RP-9
RP-10
DSC , W/g ---> exo
T , oC
2 K/min
5 K/min
10 K/min
15 K/min
20 K/min
30 K/min

Fig. 3.

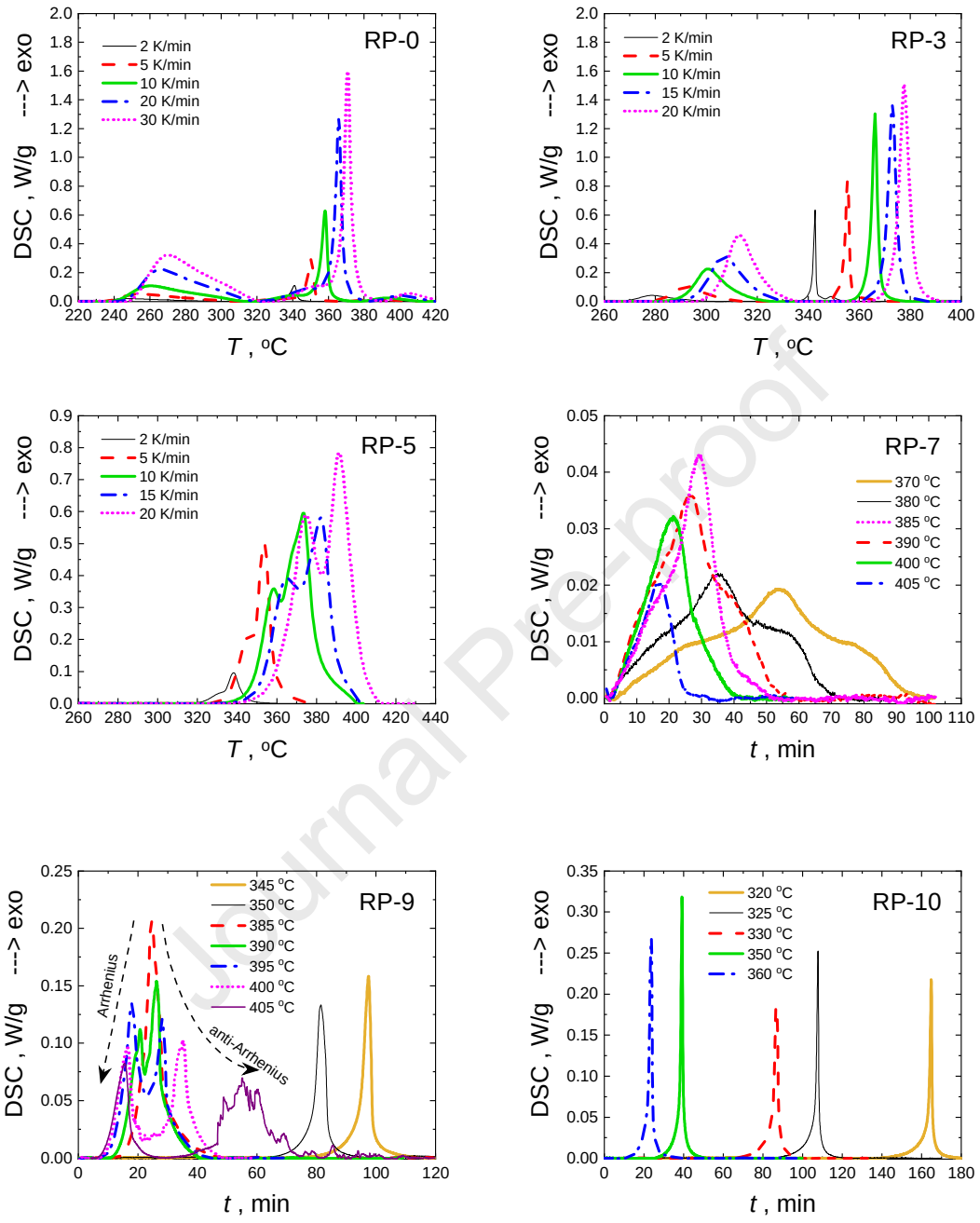

Fig. 4.

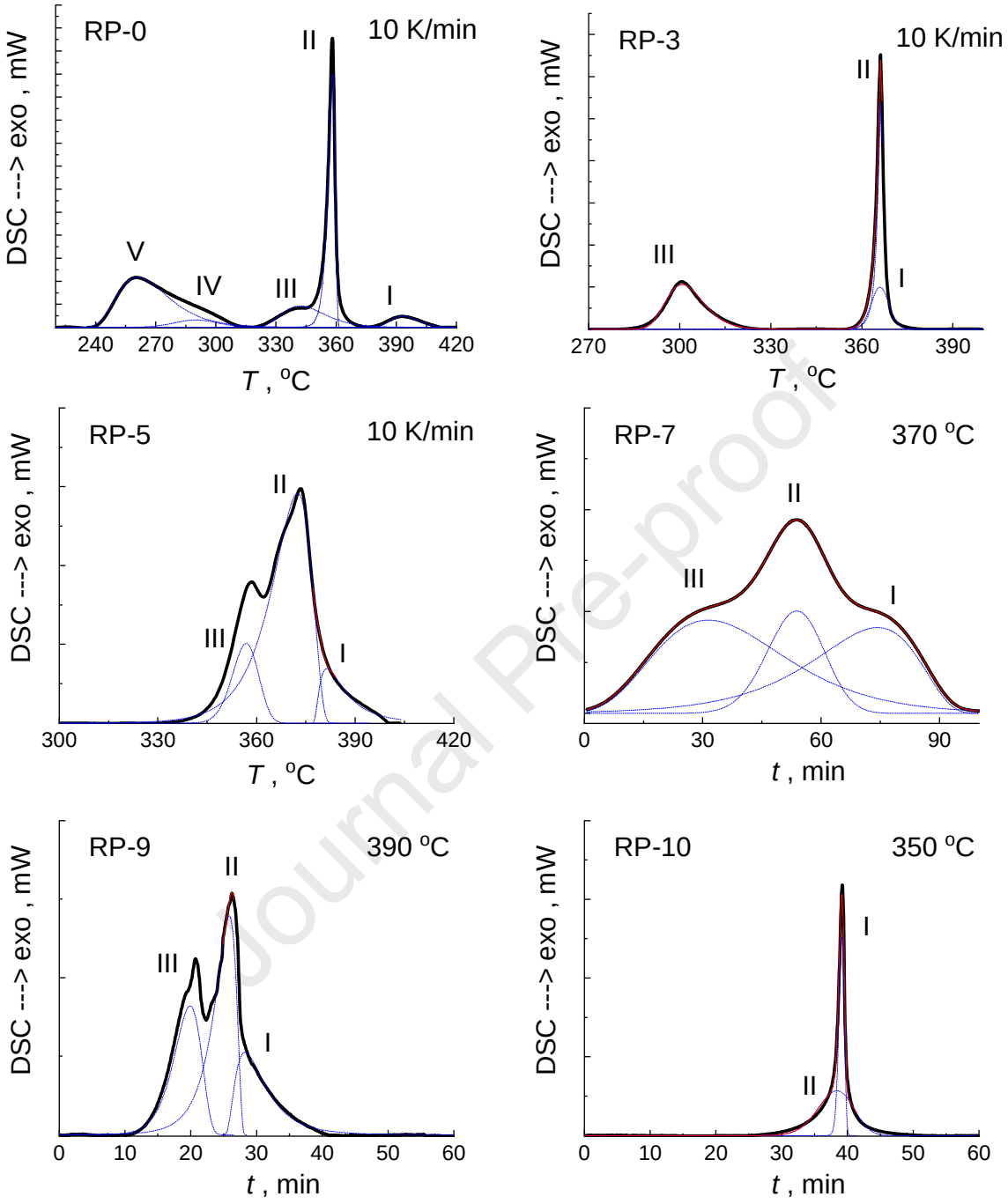

Fig. 5.

Highlights

Crystallization kinetics of novel $Bi_xGa_5Ge_{20}P_{10-x}Se_{45}Te_{20}$ glasses are studied.

Non-isothermal and isothermal crystallization kinetics are investigated.

Substitution of P with Bi in glass composition leads to a decrease in optical gap.

The anti-Arrhenius behaviour is observed and expained.

Declaration of interests

☒ The authors declare that they have no known competing financial interests or personal relationships that could have appeared to influence the work reported in this paper.

☐The authors declare the following financial interests/personal relationships which may be considered as potential competing interests: